geoconvention
Calgary • Canada • May 11-13 2026

Synthetic LF-DAS Waterfall Signatures from Poroelastic XFEM–CZM Hydraulic Fracture Simulations

Ran Tao, Juliana Y. Leung, Samer Adeeb
Department of Civil & Environmental Engineering, University of Alberta, Canada

Summary

Low frequency distributed acoustic sensing is widely used to detect and characterize hydraulic fractures by capturing fracture hits and the associated strain response around the fracture. However, interpreting field LF-DAS waterfall responses remains challenging because subsurface complexity and the coupled effects of fracture growth, poroelastic deformation, and sensing geometry often produce non-unique signatures. Prior forward-modeling studies have reproduced key LF-DAS waterfall attributes using displacement discontinuity method (DDM) representations. In this study, the hydraulic fracture is modeled in Abaqus using an extended finite element method combined with cohesive zone model (XFEM-CZM) formulation, enabling fracture initiation and propagation without prescribing a fixed fracture path. A single-fracture base case is first benchmarked against published LF-DAS signatures by (Liu et al., 2020), focusing on fracture hit timing, extending zone evolution and asymmetric patterns relative to the fracture location; and sensitivity analyses are performed to quantify how key fracture and reservoir parameters modify the waterfalls. The workflow is then extended to multi-fracture scenarios to examine how injection sequencing reshapes waterfall morphology through fracture competition and interaction, providing practical guidance for interpreting sequence-dependent stimulation responses.

1. Introduction

Low-frequency distributed acoustic sensing (LF-DAS) in offset monitor wells is increasingly used for diagnosing fracture hits and far-field fracture evolution, typically presented as real time waterfall plots(Jin & Roy, 2017; Karrenbach et al., 2017; Ugueto et al., 2019). Despite this potential, interpreting field LF-DAS waterfalls remains challenging. The observed patterns are affected by subsurface heterogeneity, measurement noise and resolution, and the coupled influences of fracture propagation, poroelastic deformation, and sensing geometry, which can lead to non-unique signatures (Liu et al., 2020).

Physics-based forward modelling is therefore essential for improving interpretability by linking observable LF-DAS features to underlying fracture evolution and interaction mechanisms. Several studies have demonstrated that simulated strain or strain-rate responses along a monitor well can reproduce representative LF-DAS signatures and provide constraints on fracture-hit timing and deformation evolution in multi-cluster settings(Sherman et al., 2019). Many existing LF-DAS forward models adopt

displacement discontinuity method fracture representations for computational efficiency (Crouch, 1976; Wu & Olson, 2015). The limitation of these approaches often relies on simplified fracture geometries or prescribed growth paths when extended to more complex interaction scenarios. In contrast, the extended finite element method represents discontinuities without prescribing a fixed trajectory, as introduced by Belytschko and Black (1999). When combined with cohesive-zone modeling, XFEM–CZM offers a practical framework for simulating fracture initiation and propagation in a solution-determined manner within a coupled poroelastic setting.

In this study, we develop a coupled Abaqus XFEM–CZM workflow that correlate hydraulic fracture propagation with synthetic LF-DAS waterfalls. Using a published single-fracture case as a benchmark, we generate an updated set of synthetic LF-DAS waterfalls within an XFEM–CZM finite-element framework and reassess the interpretation-relevant signature features reported in the literature. A parameter sensitivity study is then conducted to identify dominant fracture, reservoir, and processing controls on waterfall morphology and to establish a robust baseline for interpretation. Building on the validated baseline, the framework is extended to multi-fracture treatments to examine how injection sequencing alters fracture competition and reshapes LF-DAS waterfall responses, providing a physics-based basis for interpreting sequence-dependent stimulation behavior.

2. Novel

This work contributes an Abaqus XFEM–CZM based LF-DAS forward-modeling implementation that allows the fracture propagation path to be determined by the solution and produces synthetic waterfall responses from strain and strain rate along a monitor well. Using a published benchmark case, we generate an updated set of synthetic LF-DAS waterfalls within this XFEM-CZM framework to provide an independent comparison with prior forward-modeling results and to reassess the key signature features used in interpretation.

3. Method

3.1 XFEM-based Cohesive Fracture Modelling

3.1.1 XFEM Approximation

The Extended Finite Element Method (XFEM), introduced by Belytschko and Black (1999), extends conventional FEM by using partition of unity to incorporate local enrichment functions into the approximation. The enrichment functions typically consist of near-tip asymptotic functions that capture the singularity around the crack tip and a discontinuous function that represents the jump in displacement across the crack surfaces. The displacement vector $\mathbf{u}$ can be approximated as:

$$\mathbf{u} = \sum_{I=1}^{N} N_I(x)\left[\mathbf{u_I} + H(x)\mathbf{a_I} + \sum_{a=1}^{4} F_\alpha(x)\mathbf{b_I^a}\right], \quad (1)$$

where $N_I(x)$ is the traditional nodal shape functions, $\mathbf{u_I}$ is the traditional nodal displacement vector associated with the continuous part of the finite element solution; the second term is the product of the nodal enriched degree of freedom vector, $\mathbf{a_I}$, and the associated discontinuous jump function $H(x)$ across the crack surfaces; and the third term is the product of the nodal enriched degree of freedom vector, $\mathbf{b_I^a}$, and the associated elastic asymptotic crack-tip functions, $F_\alpha(x)$. The first term on the right-hand side applies to all the nodes in the model; the second term is valid for nodes whose shape function support is cut by the crack interior; and the third term is used only for nodes whose shape function support is cut by the crack tip. Note that although the asymptotic crack-tip enrichment functions $F_\alpha(x)$ appear in the theoretical formulation, ABAQUS does not utilize them when modelling crack propagation. Elements are either fully cracked or uncracked, this simplification enhances numerical stability but limits the ability to gradual damage evolution. Figure 1 shows normal and tangential coordinates for a smooth crack,

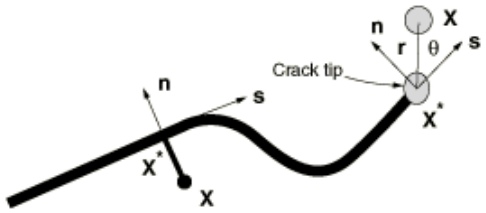


Figure 1: Extended finite element method (XFEM) approach (ABAQUS 2016 guide).

The discontinuous jump function across the crack surfaces, $H(x)$, is given by:

$$H(x) = \begin{cases} 1 & \text{if } (x - x^*) \cdot n \geq 0 \\ -1 & \text{otherwise} \end{cases}, \tag{2}$$

where x is a sample (Gauss) point, x^* is the point on the crack closest to x, and n is the unit outward normal to the crack at x^*. $F\alpha(x)$ illustrates the asymptotic crack tip functions in an isotropic elastic material, which are given by:

$$F_\alpha(r,\theta) = \left[\sqrt{r}\sin\frac{\theta}{2},\ \sqrt{r}\cos\frac{\theta}{2},\ \sqrt{r}\sin\theta\sin\frac{\theta}{2},\ \sqrt{r}\sin\theta\cos\frac{\theta}{2} \right], \tag{3}$$

where $(r,\ \theta)$ is a polar coordinate system with its origin at the crack tip and $\theta = 0$ is tangent to the crack at the tip.

3.1.2 Damage Initiation and Propagation Criteria

The fracture propagation behaviour is described by a cohesive zone model (CZM) with a linear traction-separation law, as shown in Figure 2 (Shahzamanian et al., 2021). In the present model, fracture propagates when the cohesion traction vanishes signaling the complete separation of the crack surfaces.

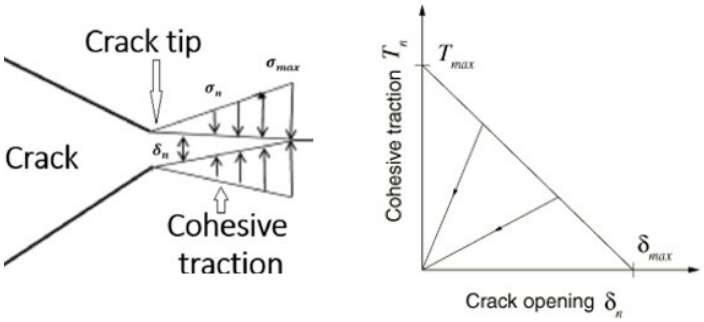


Figure 2: Traction separation law (Shahzamanian et al., 2021).

The damage initiation criterion is based on the maximum principal stress criterion, where we anticipate damage initiation at a specific point when the maximum eigenvalue of the stress matrix (maximum principal stress) reaches a critical value, equal to or greater than a threshold value—in this instance, the tensile strength τ_c of the rock. The rock will behave in a linear elastic manner before the fracture initiates.

$$f = \left\{ \frac{\langle \sigma_{\max} \rangle}{T_{\max}} \right\}, \tag{4}$$

where $\sigma_{\max}$ is the maximum principal stress at a given point, $T_{\max}$ is the tensile strength of the material, and the symbol $\langle \cdot \rangle$ used in the above equation represents the Macaulay bracket with the usual interpretation. The Macaulay brackets are used to sign if a pure compressive deformation or stress state does not initiate damage. When $f \geq 1$, fracture is initiated.

After damage initiates, the degradation of cohesive stiffness is characterized by a scalar damage variable D, which controls the gradual reduction of the normal traction from T_n to zero. The damage variable D initially equals zero and increases monotonically with further loading, reaching a value of one upon complete failure.

$$T_n = (1 - D) \cdot T_{\max}, \tag{5}$$

The value of D evolves from 0 (undamaged) to 1 (fully damaged) as the crack opening displacement δ increases form the onset separation δ_0 to the final separation $\delta_{\max}$. Under a linear softening law, the fracture energy G_c dissipated during failure is equal to the area under the traction-separation curve:

$$G_c = \frac{1}{2} T_{\max} \delta_{\max}, \tag{6}$$

In the finite element commercial software ABAQUS, the built-in MAXPS criterion (*Damage Initiation, Maxps) is used to model the onset of fracture, while the crack propagation is governed by the energy-based damage evolution law (*Damage Evolution, Type=Energy), which defines the fracture energy dissipation during separation.

3.2 Boundary Conditions and Coupled Weak Form

In this study, a two-dimensional hydraulically driven fracture is modeled within a homogeneous porous elastic medium Ω under plane strain conditions. Fracture propagation is induced by injecting an incompressible Newtonian fluid at a constant volumetric rate Q at a fixed location along the fracture. The process is assumed to be quasi-static and fully saturated, meaning the injected fluid entirely always fills the fracture, with no fluid lag at the crack tip. The boundary Γ is a union set of displacement boundary Γ_u traction boundary Γ_t, and crack surface Γ_c. There are $\Gamma_u \cup \Gamma_t \cup \Gamma_c = \Gamma$ and $\Gamma_u \cap \Gamma_t = \varnothing$.Thus, the boundary conditions of porous solid are given by

$\mathbf{u} = \bar{\mathbf{u}}$, on Γ_u,

$\boldsymbol{\sigma} \cdot \mathbf{n} = \bar{\mathbf{t}}$, on Γ_t,

$\boldsymbol{\sigma} \cdot \mathbf{n}^- = -\boldsymbol{\sigma} \cdot \mathbf{n}^+ = \mathbf{p}^+ = -\mathbf{p}^- = \mathbf{p}$, on Γ_c,

where $\mathbf{n}$ is the normal direction to the related boundary, $\bar{\mathbf{u}}$ is the given displacement on Γ_u, $\bar{\mathbf{t}}$ is the given traction on Γ_t, and $\mathbf{p}$ is the fluid pressure on Γ_c. Since the hydraulic fracture opening width is very small, it can be assumed that $\mathbf{n}^+ = -\mathbf{n}^- = \mathbf{n}$. The crack opening displacement $\mathbf{w}$ is given by:

$$\mathbf{w} = \mathbf{n} \cdot (\mathbf{u}_c^+ - \mathbf{u}_c^-), \tag{7}$$

So, the weak form of the mechanical equilibrium equation is expressed by writing the principle of virtual work:

$$\int_\Omega \boldsymbol{\sigma} : \delta\varepsilon d\Omega = \int_\Omega \rho \boldsymbol{g} \cdot \delta\mathbf{u} d\Omega + \int_{\Gamma_t} \bar{\mathbf{t}} \cdot \delta\mathbf{u} d\Gamma + \int_{\Gamma_c} \mathbf{p} \cdot \delta\mathbf{w} d\Gamma, \tag{8}$$

where $\delta\mathbf{u}$ is virtual displacement, $\delta\varepsilon$ is the virtual strain. The weak form of the mass conservation equation for a compressible pore fluid in a saturated porous medium (Eq.6) can be written as:

$$\int_\Omega \delta p \left(\frac{1}{J}\frac{\partial}{\partial t}(J\rho_w n_w) + \nabla \cdot (\rho_w n_w \mathbf{v}_w)\right) d\Omega = 0, \tag{9}$$

Similarly, the following weak form for the fluid flow within the fracture (Eq.9) can be written as:

$$\int_{\Gamma_c} \delta p_f \left(\frac{\partial w}{\partial t} + \nabla \cdot \boldsymbol{q}_f + (q_t + q_b) d\Gamma = \int_{\Gamma_c} \delta p_f Q(t) \delta(x, y) d\Gamma\right), \tag{10}$$

where δp is the virtual pore pressure field, δp_f is the virtual fracturing pressure field.

4.Results and Discussion

4.1 Model Setup and Validation

The base-case model setup follows the well configuration and treatment conditions reported by Liu et al. (2020). A single hydraulic fracture is initiated from the treatment well and propagates toward three offset monitor wells (Figure 3). All key model inputs and boundary conditions used for the benchmark, including geomechanical properties, in-situ stresses, injection schedule, fluid viscosity, and leak-off coefficient, are adopted from the published study to ensure a consistent comparison framework. This benchmark configuration provides a controlled, single-fracture reference for validating the fracture-growth response before interpreting the corresponding synthetic LF-DAS waterfalls.

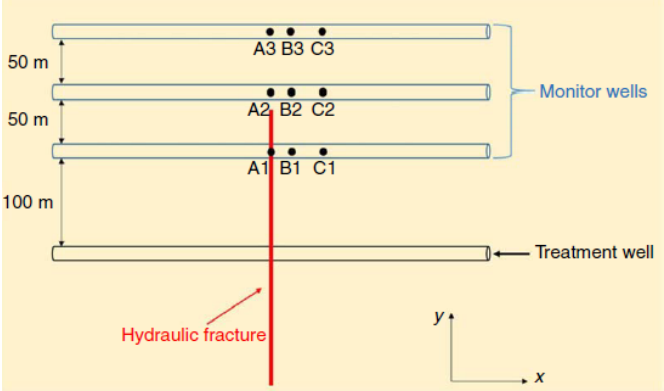


Figure 3:Schematic of well locations

Figure 4 compares fracture-length evolution predicted by three approaches: (1) an analytical solution representative of the toughness leak-off dominated regime; (2) the Abaqus XFEM-CZM result obtained in this study; and (3) the reference curve digitized from Liu et al. (2020). The XFEM–CZM prediction closely follows the analytical trend over the 3600s and remains consistent with the published benchmark curve. The overall agreement indicates that the coupled XFEM–CZM implementation reproduces the expected fracture growth behavior in this regime. Overall, these results support the use of the present XFEM–CZM workflow as a verified single-fracture baseline for subsequent LF-DAS waterfall analysis and parameter sensitivity studies.

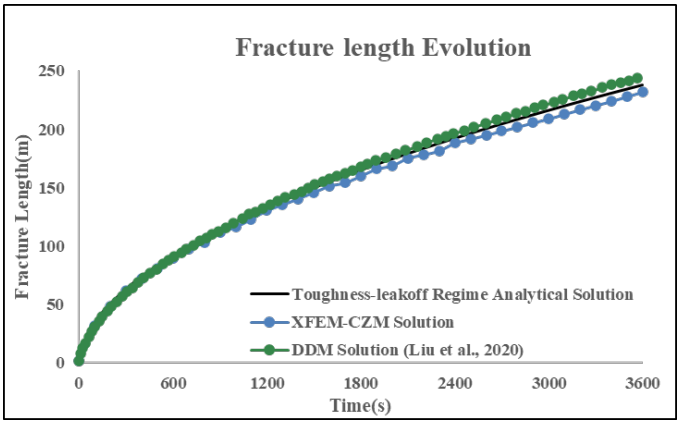


Figure 4: Fracture half-length as a function of injection time

4.2 Synthetic LF-DAS Waterfall Plots

Figure 5 presents synthetic waterfall plots extracted along three offset monitor wells located at stand-off distances of 100 m (MW1), 150 m (MW2), and 200 m (MW3). Axial strain and axial strain rate are shown as functions of time and along-well position. Across all three wells, the waterfalls evolve systematically as the fracture approaches the monitor wells, followed by a distinct change in response character once the fracture reaches the monitor-well location. This transition provides a practical reference for comparing onset timing and subsequent signature evolution across different offsets.

The strain waterfalls show a localized deformation response near the fracture location that evolves in both amplitude and spatial extent with injection time. Consistent offset-dependent trends are observed: MW1 exhibits earlier onset and stronger localization, whereas MW2 and MW3 show delayed onset with comparatively reduced intensity and a narrower affected region. The strain-rate waterfalls emphasize transient behavior by highlighting changes between successive time steps and provide a clearer delineation of onset and time-dependent evolution near the fracture position. With continued injection, the localized strain-rate response trends toward a more stable pattern. Overall, the XFEM–CZM results reproduce the main qualitative LF-DAS features used for interpretation, including onset timing, localization near the fracture position, and systematic dependence on monitor-well offset, supporting this workflow as an alternative way for generating interpretation-oriented synthetic LF-DAS observables.

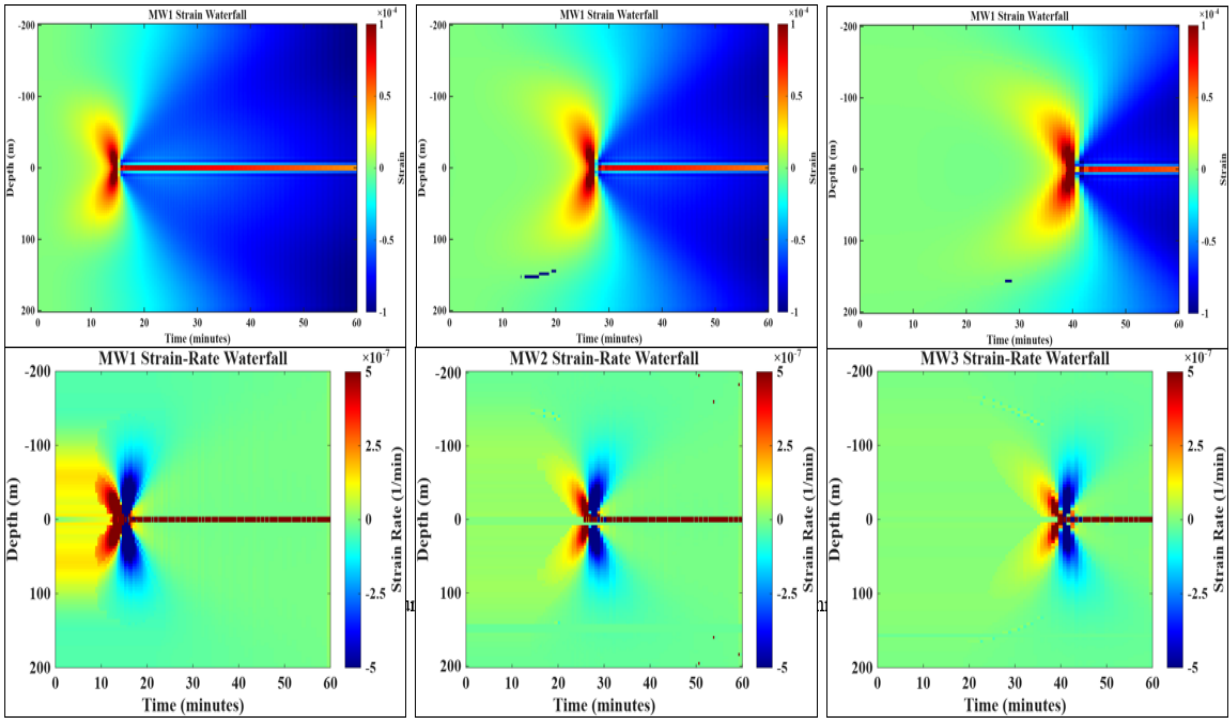


Figure 5:Waterfall plots of strain and strain rate along three monitor wells for base case.

5.Conclusion

This work develops an Abaqus-based XFEM–CZM forward modeling workflow that correlates hydraulic fracture propagation to synthetic LF-DAS waterfall generation along offset monitor wells. For a published single-fracture benchmark configuration, the XFEM–CZM results produce strain and strain-rate waterfall patterns that are qualitatively consistent with reported LF-DAS signatures and exhibit systematic trends with monitor-well offset distance. These results indicate that XFEM–CZM can serve as a practical framework for constructing synthetic LF-DAS observables without prescribing a fixed fracture path. The established single-fracture baseline provides a foundation for ongoing sensitivity analyses and subsequent extensions to multi-fracture scenarios aimed at crack interaction and sequencing effects on LF-DAS waterfall morphology.

Acknowledgements

The authors gratefully acknowledge the supervision and guidance of Dr. Samer Adeeb and Dr. Juliana Leung throughout this research. Their expertise hydraulic fracturing significantly contributed to the development of this work. The numerical simulations were conducted using the ABAQUS software.

References

Belytschko, T., & Black, T. (1999). Elastic crack growth in finite elements with minimal remeshing. *International Journal for Numerical Methods in Engineering*, *45*(5), 601-620. https://doi.org/https://doi.org/10.1002/(SICI)1097-0207(19990620)45:5<601::AID-NME598>3.0.CO;2-S

Crouch, S. L. (1976). Solution of plane elasticity problems by the displacement discontinuity method. I. Infinite body solution. *International Journal for Numerical Methods in Engineering*, *10*(2), 301-343. https://doi.org/https://doi.org/10.1002/nme.1620100206

Jin, G., & Roy, B. (2017). Hydraulic-fracture geometry characterization using low-frequency DAS signal. *The Leading Edge*, *36*(12), 975-980. https://doi.org/10.1190/tle36120975.1

Karrenbach, M., Ridge, A., Cole, S., Boone, K., Kahn, D., Rich, J., Silver, K., & Langton, D. (2017). DAS Microseismic Monitoring and Integration With Strain Measurements in Hydraulic Fracture Profiling. SPE/AAPG/SEG Unconventional Resources Technology Conference,

Liu, Y., Wu, K., Jin, G., & Moridis, G. (2020). Rock Deformation and Strain-Rate Characterization during Hydraulic Fracturing Treatments: Insights for Interpretation of Low-Frequency Distributed Acoustic-Sensing Signals. *SPE Journal*, *25*(05), 2251-2264. https://doi.org/10.2118/202482-pa

Shahzamanian, M. M., Lin, M., Kainat, M., Yoosef-Ghodsi, N., & Adeeb, S. (2021). Systematic literature review of the application of extended finite element method in failure prediction of pipelines. *Journal of Pipeline Science and Engineering*, *1*(2), 241-251. https://doi.org/10.1016/j.jpse.2021.02.003

Sherman, C., Mellors, R., Morris, J., & Ryerson, F. (2019). Geomechanical modeling of distributed fiber-optic sensor measurements. *Interpretation*, *7*(1), SA21-SA27. https://doi.org/10.1190/int-2018-0063.1

Ugueto, G. A., Todea, F., Daredia, T., Wojtaszek, M., Huckabee, P. T., Reynolds, A., Laing, C., & Chavarria, J. A. (2019). Can You Feel the Strain? DAS Strain Fronts for Fracture Geometry in the BC Montney, Groundbirch. SPE Annual Technical Conference and Exhibition,

Wu, K., & Olson, J. E. (2015). A simplified three-dimensional displacement discontinuity method for multiple fracture simulations. *International Journal of Fracture*, *193*(2), 191-204. https://doi.org/10.1007/s10704-015-0023-4